NUCLEAR STRUCTURE -- EXPERIMENTAL

ELASTIC SCATTERING OF 318 MeV ^{6}Li FROM ^{12}C AND ^{28}Si

A. Nadasen,[a] J.S. Winfield, B. Ashe,[a] F.D. Becchetti,[b] J. Brown,[b] J. Brusoe,[a] D. Hotz,[b] J. Janecke,[b] D. Roberts,[b] P. Schwandt,[c] and G. Yoo

Elastic scattering of 318 MeV ^{6}Li (3+) ions from ^{12}C and ^{28}Si[1] were measured over large angular ranges with beams from the K500 cyclotron. The scattered ^{6}Li particles were detected with the S320 spectrometer (QQDM) and its standard focal plane detection system. The resolution was adequate to extract both the ground and first excited state data. The angular step and angular resolution were carefully chosen so that the shapes of the angular distributions were clearly defined.

The elastic scattering differential cross sections are shown as solid dots in Fig. 1. The data are characterized by diffractive oscillations at the forward angles. Beyond the rainbow angle one observes smooth exponential falloff, basically due to the dominance of far-side scattering. Measurement of these large-angle data is crucial for the determination of unique potentials. Optical model analyses of the data have been carried out using the code ECIS, and unique OM potential parameters (Table I) have been derived. The fits to the data are shown as solid lines in Fig. 1.

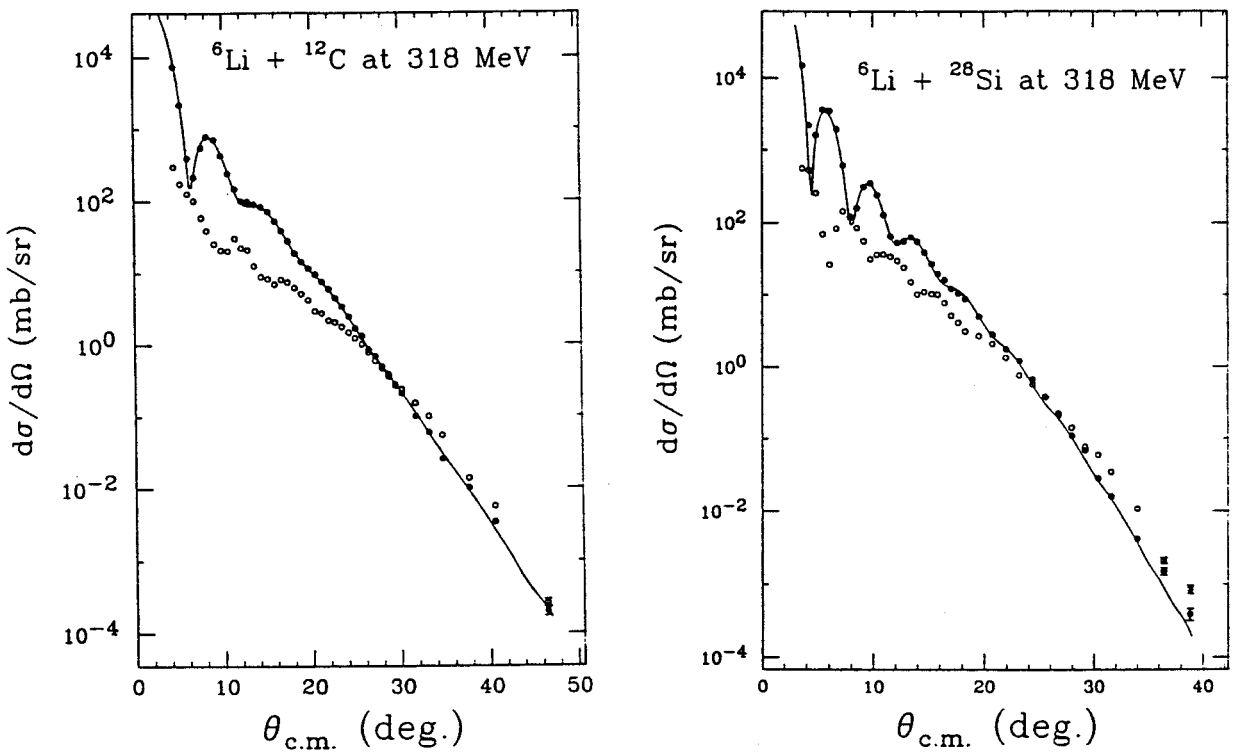

Fig. 1. Cross sections for the elastic (solid dots) and inelastic (open circles) scattering of 318 MeV ^{6}Li from (a) ^{12}C and (b) ^{28}Si. The solid curves represent calculations with the unique OM potentials.

The volume integrals of the potentials are in agreement with the $A^{1/3}$ dependence on the target nucleus derived at 210 MeV.[2] Figure 2 shows the volume integrals of the real potentials from all available investigations as a function of bombarding energy. The scatter of the lower energy data is a reflection of the ambiguities in the derived potentials. The solid lines depict the energy dependence derived with data at $E \leq 210$ MeV.[2] The values for 318 MeV in both cases (shown as open circles) are larger than expected. It is not clear whether this is a reflection of a weaker energy dependence. Further measurements are needed to clarify this issue.

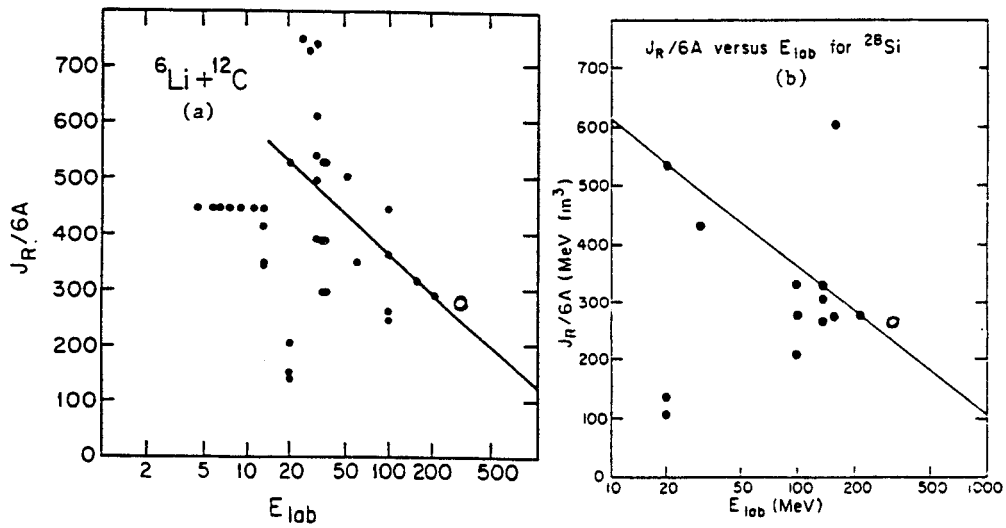

Fig. 2. Volume integrals of the real potentials for ^{6}Li scattering from (a) ^{12}C and (b) ^{28}Si as a function of beam energy. The straight lines represent the energy dependence derived with the 210 MeV data. The open circles are results at 318 MeV.

Table I: Unique OM parameters derived from the elastic scattering of 318 MeV ^{6}Li from ^{12}C and ^{28}Si.

	V	r_o	a_o	W_v	r_w	a_w	$J_R/6A$	x^2/N
^{12}C	122.5	1.144	0.902	27.6	1.706	0.914	280	2.7
^{28}Si	118.1	1.291	0.874	40.7	1.596	0.770	263	3.8

In order to understand the ^{6}Li-nucleus interaction at a more fundamental level, microscopic potential-folding model calculations are being carried out using the program Fold. Since unique phenomenological OM potentials are available, it is hoped that some insight into the causes of the 0.5 to 0.7 renormalization required for potentials generated at lower energies.[3] Effects of the Pauli exclusion principle, projectile breakup and distortions will be explored.

Inelastic cross sections leading to the first excited (2^+) states have been extracted. These are shown as open circles in Fig. 1. The shapes of the angular distributions are similar to those of elastic scattering, except for the phase difference which is due to the Blair phase rule.[4] DWBA calculations are underway in order to determine the deformation lengths, $\beta_2 R$, and quadruple moments, q_{20} and to compare them with results at 210 MeV.[5] Because of the comparatively high inelastic cross sections at large angles, coupled channels effects are expected to be important. Such calculations will also be pursued.

a. University of Michigan, Dearborn.
b. University of Michigan, Ann Arbor.
c. Indiana University Cyclotron Facility.

References

1. A. Nadasen et al., Bull. Am. Phys. Soc. 35, 1667 (1990); A. Nadasen et al., to be published.
2. A. Nadasen et al., Phys. Rev. C 37, 132 (1988); ibid. C 39, 536 (1989).
3. C.L. Woods, B.A. Brown and N.A. Jelley, J. Phys. G. 8, 1699 (1982).
4. J.S. Blair, Proc. Int. Conf. on Nuclear Structure, Kingston, ed. D.A. Bromley and E.W. Vogt, U. of Toronto Press (1960) p. 824.
5. A. Nadasen et al., Phys. Rev. C 40, 1237 (1989).

THE (^{6}Li,^{6}Li γ) TECHNIQUE AND ISOVECTOR SPIN-FLIP TRANSITIONS

J.S. Winfield, N. Anantaraman, Sam M. Austin, J. Kelley, D.J. Morrissey, A. Nadasen,[a] N. Orr, and R.M. Ronningen

The (p,p′) reaction at intermediate energies has been successful in the study of spin-transfer strength over a wide range of nuclei.[1] However, there are some drawbacks to this technique in that both isoscalar and isovector amplitudes can contribute, which generates a large background from natural parity states at high excitation. In addition, excitations of 1^+ states are made through both isoscalar and isovector $\Delta S=1$ amplitudes. The tail of the elastic peak is also a problem, making it difficult to observe low-lying strength, especially for heavy nuclei. A potential reaction that avoids the disadvantages of (p,p′) is (^{6}Li,^{6}Li′), with ^{6}Li inelastically scattered to its $J^\pi=0^+$, T=1 state at 3.56 MeV, and coincident detection of the de-excitation γ-ray from the projectile. Since the ground state of ^{6}Li is 1^+, T=0, the transitions have $\Delta S=1$, $\Delta T=1$, so that natural parity and isoscalar transitions are forbidden [this spin-isospin selectivity is similar to that of the analog charge exchange reaction (^{6}Li,^{6}He)]. Advantages of ^{6}Li over other heavy-ion projectiles include the absence of other gamma-decaying states, and the technical possibility of polarized lithium beams, permitting future studies of spin observables.

A feasibility study of the technique has been carried out with the S-320 spectrograph and an array of 8 BGO and 10 BaF_2 detectors mounted on a thin-walled dome at the usual S-320 target location. A beam of E/A=35 MeV ^{6}Li from the K500 cyclotron bombarded targets of ^{24}Mg and ^{12}C. The reaction of interest was ^{24}Mg(^{6}Li,^{6}Li′)^{24}Mg$_{10.71}$, chosen because the (1^+, T=1) state at 10.71-MeV in ^{24}Mg was prominently excited in a (p,p′) study at 201 MeV.[2] The ^{12}C target was used to set up the coincidence gate through the decay of the 4.44-MeV state and as an online calibration.

A previous exploratory study[3] had shown that the background in the γ-detectors was a critical problem. In the present experiment, measurements at two angles, 3° and 0°, were attempted. For the 3° measurement, the beam was stopped in a Faraday cup about 30% farther back from the target chamber than the usual wedge Faraday cup. Besides giving more distance between the cup and the γ-detectors, the extended wedge box allowed additional shielding. For the 0° measurement, the beam passed through the center of the S-320 detector box into a dump in the vault shielding wall. Inside the detector box, a 16-cm long gas proportional counter and three 1/4-inch thick plastic scintillators were set up on one side of the beam path. The specially-constructed gas detector is described elsewhere in this report. It was calibrated

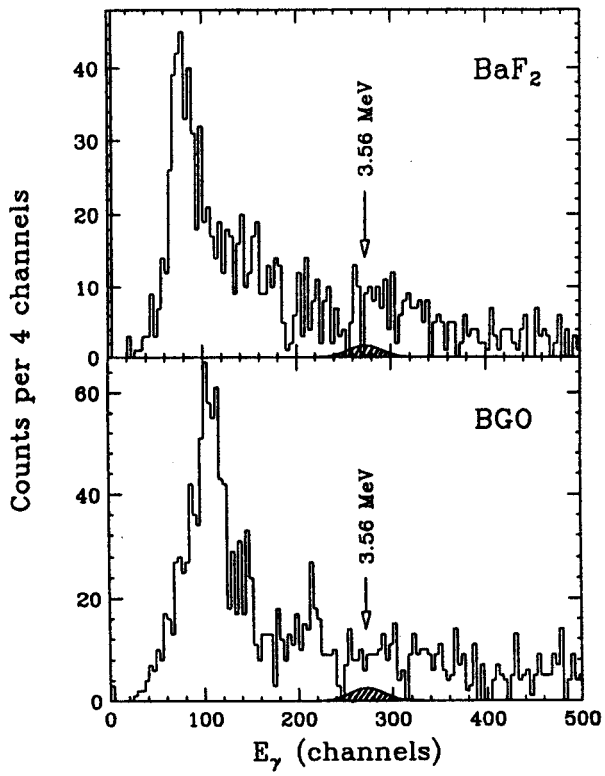

Figure 1: Summed BGO and BaF_2 energy spectra gated on the (10.71 MeV + 3.56 MeV) region of the particle spectrum. The expected location of the 3.56 MeV gamma ray is indicated by an arrow. The data are for the spectrograph set at 0°.

by scanning elastic scattering peaks across the detector and by observation of known inelastically excited states in ^{12}C and ^{24}Mg. The first two scintillators were used to measure energy-loss and residual energy, while the third was used to veto light particles.

The total solid angle covered by the BGO (BaF_2) detectors was 1.06 sr (0.67 sr). The photopeak efficiencies, measured off-line with sources at the target location, ranged from 0.25 to 0.33. A wall of lead bricks, iron-loaded concrete, and paraffin wax shielded the γ-detectors from the 3° Faraday cup. In the 3° configuration, the ratio of rates in the γ-detectors for target-in:target-out was approximately 1.6:1. By comparing the target-in rates for the two angles, we deduce that the γ-background rate was about five times lower at 0° than at 3°. In order to keep the raw counting rates in individual γ-detectors below 15 kHz, it was necessary to limit the beam current to a few nA. This suggests that a higher granularity array may be desirable.

During the experiment, a coincidence was required between an S320 event and any of the BGO's or BaF_2's. In the off-line playback, separate passes were made through the data to select events associated with the same cyclotron rf pulse as the detected ^{6}Li (real + random coincidences) and those associated with subsequent pulses (purely random coincidences). The latter were then subtracted from the former. The ratio of reals to randoms was about 4:1 at both spectrograph angles.

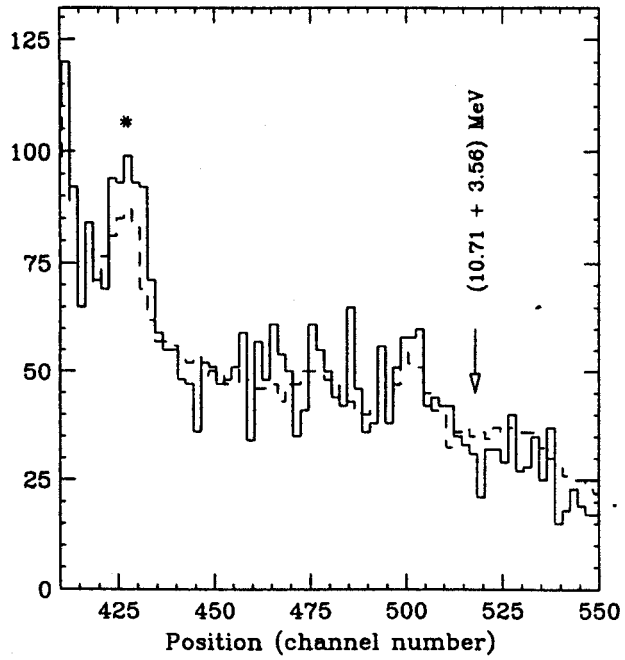

Figure 2: Focal plane spectra taken at 3°. The solid histogram is gated on the region of 3.56 MeV in the gamma spectra. The dashed histogram has no software gamma gates (but was taken with the coincidence trigger). and is roughly scaled to match the gated one. The peak labeled ($\star$) is identified as the 8.36 MeV 3^- state in ^{24}Mg.

The calibrated gamma signals had to be corrected for the Doppler shift of the 3.56 MeV-γ emitted from the moving ^{6}Li. To look for the 3.56 MeV γ-rays, a gate was set on the region of the particle spectrum corresponding to an excitation energy of 10.71 MeV plus 3.56 MeV. The result for the 0° run is shown in Fig. 1.

The expected yields [estimated from the (^{6}Li,^{6}He) cross section[4]] are shown in the figure as Gaussians with widths equal to the experimental resolution. The "background" (which presumably arises from target γ-rays) seems too high to observe the 3.56 MeV signal. The prominent peak at the left of the spectrum corresponds to falsely Doppler-shifted 1.37–MeV and 1.63–MeV γ-rays from ^{24}Mg($2^+ \rightarrow 0^+$) and ^{20}Ne($2^+ \rightarrow 0^+$), respectively (the threshold for ^{24}Mg $\rightarrow$ ^{20}Ne + α is 9.31 MeV).

As might be expected from the γ-spectrum, when the particle spectrum is gated on the 3.56 MeV

γ-rays from the de-excitation of ^{6}Li, no enhancement of the particle spectrum in the energy region of (10.71 MeV + 3.56 MeV) was observed (Fig. 2). This result shows that contributions from target γ-rays are an unavoidable complication for such experiments. A straightforward approach to deal with them would obtain a measure of the strength of the target γ-ray contribution by setting gates on either side of the Doppler-shifted 3.56-MeV peak and subtract the events associated with target γ-ray emission from the particle spectrum. This was not attempted for the present data because of the poor statistics.

Requirements to perform these experiments with precision would be a large solid angle spectrograph, a high granularity γ-detector array covering large solid angle, and the best possible γ-energy resolution to reduce the contribution from target γ-rays. Higher bombarding energies, leading to smaller momentum transfer, would probably be advantageous, since the spin selectivity of the reaction would be improved.

a. Univ. of Michigan, Dearborn, MI.

References

1. C. Djalali, *et al.*, Nucl. Phys. A410, (1983), p 399.
2. G.M. Crawley, C. Djalali, N. Marty, M. Morlet, A. Willis, N. Anantaraman, B.A. Brown, and A. Galonsky, Phys. Rev. C39, (1989), p 311.
3. N. Anantaraman, *et al.*, NSCL Annual report, 1987, p. 36.
4. J.S. Winfield, N. Anantaraman, Sam M. Austin, Z. Chen, A. Galonsky, J. van der Plicht, H.-L. Wu, C.C. Chang, and G. Ciangaru, Phys. Rev.C35, (1987), p 1734.

(^{12}C,^{12}B) AND (^{12}C,^{12}N) REACTIONS AT E/A = 70 MeV AS SPIN PROBES: CALIBRATION AND APPLICATION TO 1^+ STATES IN ^{56}Mn

N. Anantaraman, J.S. Winfield, S.M. Austin, C. Djalali, J.A. Nolen, Jr., A. Gillibert,[a] W. Mittig,[a] Zhan Wen Long,[a] and J.A. Carr[b]

As reported in the 1989 Annual Report, angular distributions were measured at Laboratoire GANIL for $0^+ \rightarrow 1^+$ transitions with the (^{12}C,^{12}B) reaction on targets of ^{12}C, ^{26}Mg, ^{54}Fe, ^{58}Ni, and ^{90}Zr and with the (^{12}C,^{12}N) reaction on targets of ^{12}C and ^{56}Fe. The bombarding energy was E/A = 70 MeV, and small-angle data were obtained. In last year's report, a preliminary empirical calibration curve for $\hat{\sigma}$, the cross section per unit Gamow-Teller (GT) strength B(GT), as a function of target mass, was presented. It was obtained by studying (^{12}C,^{12}B) transitions to states whose B(GT) values are known. The idea was that, if a consistent result is obtained, then one can use this curve to determine B(GT) from the charge-exchange cross section measured for an unknown transition. The scatter of the calibration measurements about the curve provides a measure of the accuracy of the procedure. In this report, we present the final calibration curve we have determined and apply it to obtain B(GT) values of astrophysical interest for two low-lying 1^+ levels in ^{56}Mn from the cross sections measured for the ^{56}Fe(^{12}C,^{12}N)^{56}Mn reaction. The results are compared with two shell-model calculations performed to obtain B(GT) for ^{56}Fe $\rightarrow$ ^{56}Mn transitions and with another calculation from the literature.

A comparison of the measured cross sections with the results of distorted-wave approximation (DWA) calculations shows that $0^+ \rightarrow 1^+$ transitions are predominantly one-step at the bombarding energy of E/A = 70 MeV. The calculated cross sections are generally in good agreement with the measured cross sections, requiring renormalizations that are typically less than 40%, which is in the range of the overall calculational and experimental uncertainties. In many cases the angular distributions are well described quantitatively.

The following procedure was used to obtain the unit cross section, the ratio of the experimental cross section extrapolated to q = 0 to the GT strength B(GT). First, DWA calculations were done to provide L = 0 and L = 2 angular distributions. The relative strengths of these distributions were adjusted to yield an optimal fit to the cross section, corresponding to a minimum in X^2. This yielded the L = 0 cross section at 0°, i.e. at zero transverse momentum transfer. In order to obtain the cross section corresponding to zero total momentum transfer (q = 0), this cross section was multiplied by the ratio, F(Q), of the L = 0 cross section calculated at Q = 0 to that at

the actual Q of the reaction (typically around -20 to -30 MeV). Dividing this cross section by the corresponding B(GT) gives $\hat{\sigma}$, the cross section per unit GT strength. The results are plotted in Fig. 1. The dashed and the dot-dashed curves shown in Fig. 1 were obtained assuming a linear and a quadratic form, respectively, for the A-dependence of $\hat{\sigma}$. These assumptions were made in the absence of any theoretical input as to the A-dependence. The parameters of the fits, determined by least-squares fittings in which the data points were weighted by their relative uncertainties, are:

$\hat{\sigma}$ = (4.078±0.390) - (0.0382±0.006)A (linear fit);

$\hat{\sigma}$ = (6.275±0.794) - (0.134±0.030)A + [(0.814±0.256)/1000]A^2 (quadratic fit).

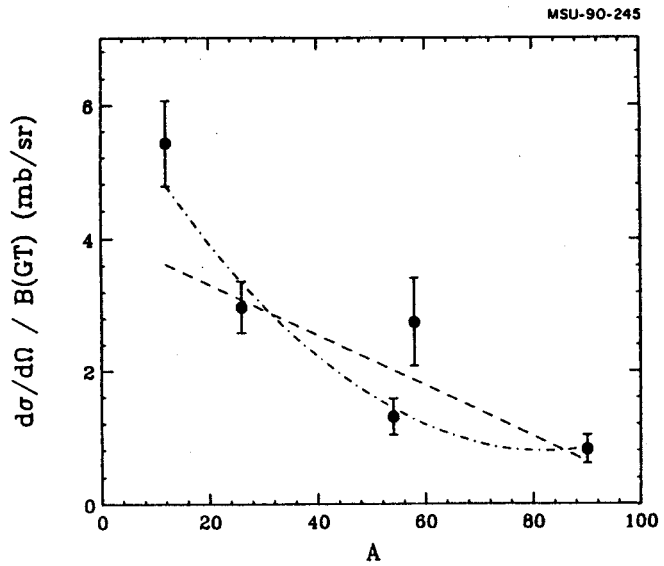

Fig. 1. Calibration curves determined from the (^{12}C,^{12}B) reaction on several nuclei at E/A = 70 MeV, as described in the text. The dashed and dot-dashed curves represent a linear and a quadratic fit, respectively.

The calibration curves thus determined are essentially phenomenological in nature and not dependent on detailed reaction calculations; for example, they are relatively insensitive to the choice of optical potentials used to extrapolate to q=0, since that procedure involves only the ratio of two calculated cross sections. They were used to obtain β^+ GT strengths from the cross sections measured for the ^{56}Fe(^{12}C,^{12}N)^{56}Mn reaction.

Figure 2 shows spectra for the ^{56}Fe(^{12}C,^{12}N)^{56}Mn reaction. In the forward angle spectra, besides the H(^{12}C,^{12}N)n contaminant peak, two sharp and cleanly-resolved peaks are observed. From the focal plane calibration, we estimate the excitation energies in Mn for these peaks to be 0.025±0.15 MeV and 1.20±0.26 MeV. By comparison with the (t,^{3}He) spectrum of Azjenberg-Selove et al.,[1] and assuming that the spins of the states we observe are 1^+, we identify these states with the 0.11 MeV and 1.17 MeV levels in ^{56}Mn. The hydrogen contaminant in the target interferes with the low-lying Mn states for scattering angles from about 0.3° to 1.3°. Scaling the hydrogen peak in the 0.05° spectrum from the $(CH_2)_n$ target to the corresponding peak in the ^{56}Fe spectrum permitted an accurate subtraction of the hydrogen peak in the ^{56}Fe spectra. This was a significant correction only for

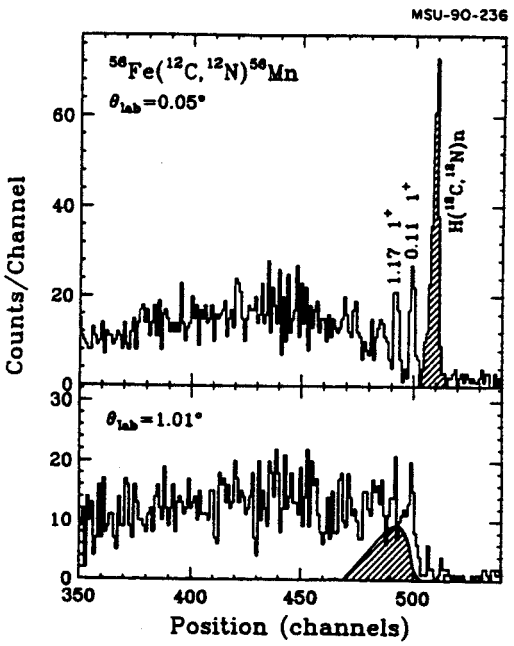

Fig. 2 Spectra for ^{56}Fe(^{12}C,^{12}N)^{56}Mn at E/A = 70 MeV. The contribution due to the reaction on the H contaminant in the target is shaded. The angular bin widths are ±0.24°.

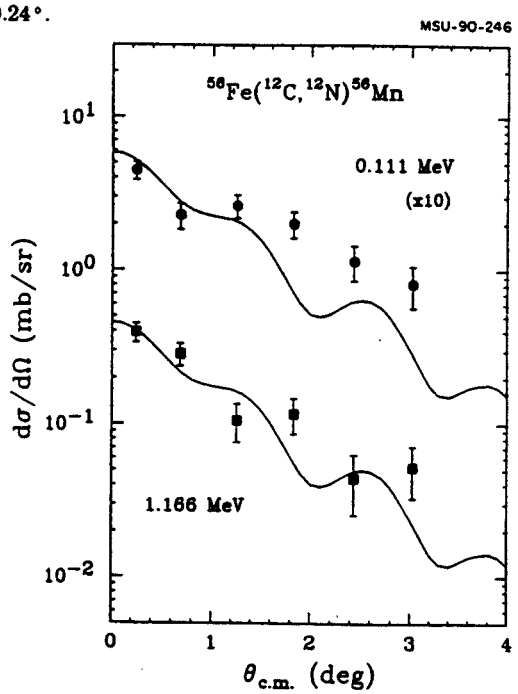

Fig. 3. Angular distributions for the ^{56}Fe(^{12}C,^{12}N)^{56}Mn reaction at E/A = 70 MeV, leading to two 1^+ states. The curves represent results of DWA calculations normalized to the data.

laboratory angles of 0.53° and 1.01°. The spectra were then binned over a ±0.24° range and analyzed by making multiple Gaussian peak fits. Inspection of Fig. 2 shows that, with the energy resolution achieved, no other states are resolved.

The angular distributions for the two isolated 1^+ states are shown in Fig. 3, along with the results of DWA calculations normalized to the data. The DWA calculations used shell-model wave functions we calculated. Next, a multipole decomposition of the two angular distributions was done in the manner described above. The normalizations N'(L=0) and N'(L=2) thus obtained show that the transition to the 0.11-MeV state has more L = 2 strength than predicted with the shell-model wave functions used, whereas that for the 1.17-MeV state is correctly predicted as regards the relative L = 0 and L = 2 contributions. From the L = 0 cross section data, $\sigma(L=0,\theta=0,Q=0)$ values for the two transitions were obtained in the same way as described above. To convert them to B(GT), the unit cross section $\hat{\sigma}$ at A=56 was read off from the two calibration curves shown in Fig. 1. The values of $\hat{\sigma}$(A=56) determined by the linear and the quadratic calibrations are 1.94 and 1.35 mb/sr, respectively. The average of these was used to convert $\sigma(L=0,\theta=0,Q=0)$ to B(GT). The uncertainty in B(GT) was determined by adding in quadrature the statistical error in the measured cross

sections (±17%), the error in the procedure for extrapolating to θ=0 and Q=0 (±10%), and the uncertainty in $\hat{\theta}$ corresponding to half the difference between the linear and the quadratic fits (±18%). The B(GT) values thus obtained were then corrected for the fact that the reaction used to measure the A=56 cross sections was (^{12}C,^{12}N) whereas the calibration curves of Fig. 1 are based on data from the (^{12}C,^{12}B) reaction. Since the B(GT) values for the ^{12}C - ^{12}N and ^{12}C - ^{12}B transitions are different by 13%, the (^{12}C,^{12}N) and (^{12}C,^{12}B) cross sections are different because they scale (to first order) with the B(GT) in the projectile-ejectile system. The B(GT) values extracted for ^{56}Mn were therefore increased by 13%.

The B(GT) values obtained by the above procedure for the 1^+ states at E_x = 0.11 and 1.17 MeV in ^{56}Mn are shown in Table I, where they are compared with the results of three shell-model calculations. One of these is the calculation of Bloom and Fuller[2] and the other two are our calculations in two model spaces: a zero-order model space (a 2p2h configuration for the initial state and a 3p3h configuration for the final state) and a larger space in which 1p1h excitations in both initial and final states are included. The extracted strengths appear to agree better with our calculated results than with those of Ref. 2. The average quenching factor for the sum of the two transitions obtained by comparing the extracted strengths to Bloom and Fuller's calculation, our calculation in the smaller model space, and our calculation in the larger model space is 0.49, 0.70, and 0.75, respectively. These factors are somewhat larger than those obtained from a comparison of

Table I. Results for B(GT) values for 1^+ states in ^{56}Mn from analysis of the ^{56}Fe(^{12}C,^{12}N)^{56}Mn data and from shell-model calculations.

State	Expt		Theory A[a]		Theory B[b]	Theory C[c]
	E_x(MeV)	B(GT)	E_x(MeV)	B(GT)	B(GT)	B(GT)
1	0.11	0.65±0.17	0.24	0.26	0.88	0.83
2	1.17	0.83±0.22	1.3	2.73	1.23	1.14

[a]Reference 2. The numbers given for E_x and B(GT) do not appear in this form in Ref. 2; they were provided by S.D. Bloom.

[b]Our calculation in the smaller model space described in the text; energy spacing between the two 1^+ states is 1.26 MeV, compared to 1.06 MeV experimentally.

[c]Our calculation in the larger model space described in the text; energy spacing between the two 1^+ states is 1.45 MeV, compared to 1.06 MeV experimentally.

the results for the $^{54}Fe(n,p)^{54}Co$ reaction[3] with the calculation of Ref. 2, although the uncertainties are substantial. Calculations of the supernova process have previously been made[4] using the results of Ref. 2. It remains to be seen how these calculations will be affected by the different B(GT) values obtained in the present experiment.

The calculated B(GT) values have a significant dependence on both the two-body interaction and the model spaces involved. Further measurements such as those presented here will be required to constrain the shell-model calculations so as to facilitate reliable calculations for transitions which are important in astrophysical phenomena but which cannot be measured in the laboratory. This is particularly important because it appears that individual transitions can sometimes have an important effect in presupernova stars.[5]

a. Laboratoire GANIL, Caen, France.
b. Florida State University, Tallahassee, Florida.

References

1. F. Ajzenberg-Selove, R.E. Brown, E.R. Flynn, and J.W. Sunier, Phys. Rev. C **30**, 1850 (1984); C **31**, 777 (1985).
2. S.D. Bloom and G.M. Fuller, Nucl. Phys. **A440**, 511 (1985).
3. M.C. Vetterli et al., Phys. Rev. C **40**, 559 (1989).
4. G.M. Fuller, W.A. Fowler, and M.J. Newman, Ap. J. **293**, 1 (1985).
5. M.B. Aufderheide, G.E. Brown, T.T.S. Kuo, D.B. Stout, and P. Vogel, Ap. J. **362**, 241 (1990).

IDENTIFICATION OF NEW NUCLEI NEAR THE PROTON-DRIP LINE FOR $31 \leq Z \leq 38$

M.F. Mohar, D. Bazin, W. Benenson, D.J. Morrissey, A.C. Mueller,[a] D. Guillemaud-Mueller,[a]
N.A. Orr, B.M. Sherrill, D. Swan, J.A. Winger

The work presented is result of an experiment to produce and observe new nuclei near the proton-drip line in the mass region $50 < A < 100$. Such observations were made possible for the first time by the combination of a high energy, rare isotope beam of ^{78}Kr and the newly-commissioned A1200 beam analysis device (figure 1) at the National Superconducting Cyclotron Laboratory. The method used to produce and identify these isotopes is similar to that used by GANIL for mapping the proton-drip line below Z=30 [1] with the addition of precise rigidity information. An E/A = 65 MeV ^{78}Kr beam was produced by the K1200 Cyclotron and reacted with an enriched ^{58}Ni target, 94 mg/cm^2 thick, at the object point of the A1200. The reaction products were collected and transported through the A1200 Mass Separator to a four-element silicon detector telescope (ΔE1, ΔE2, E1, and E2) at the achromatic final image point of the device. A position sensitive parallel plate avalanche detector placed at an intermediate dispersive focal plane, labeled image #2 in the figure, and an NMR measurement of the dipole fields were used to determined the rigidity of the nuclei produced. The rigidity was calibrated by sweeping the primary beam across the dispersive image. The silicon detector telescope provided two energy loss measurements and a total energy measurement which enabled redundant Z determinations from ΔE versus E_{TOTAL} spectra. The total kinetic energy measurement was also used to determine the Q, or charge, used to calculate the mass from the particle rigidity measurement. A thin plastic scintillator start-detector was placed after the first dipole pair at image #1. The time difference between the start detector signal and the signal produced in the ΔE1 silicon detector over the 14 meter flight path were used to determine the velocity of each particle.

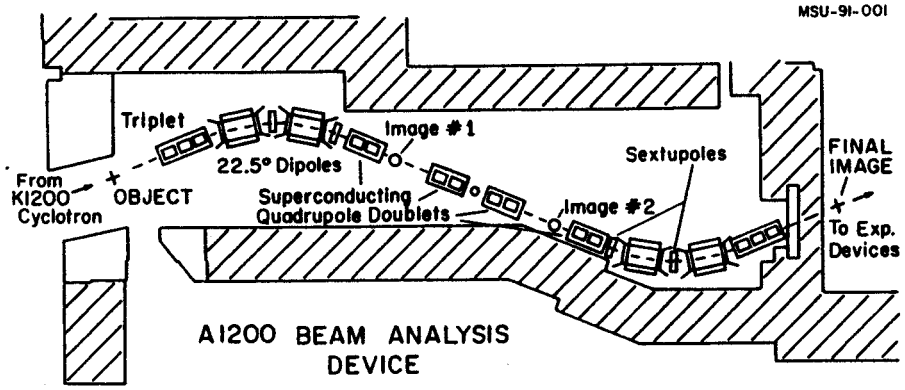

Figure 1: Schematic layout of the A1200 beam analysis device.

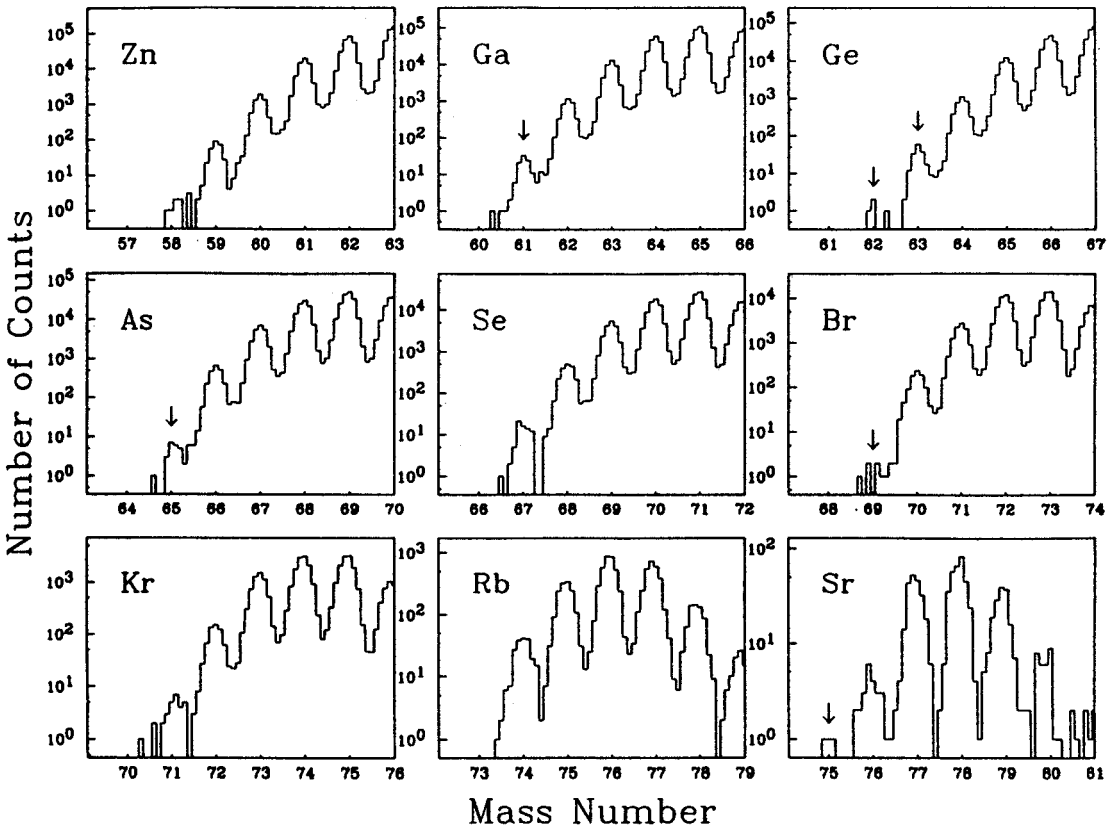

Figure 2: Mass spectra showing the number of counts in each mass peak for Z=30–38 (zinc through strontium) on a logarithmic scale. The new nuclei are indicated with arrows.

The measured parameters, rigidity, ΔE, E_{TOTAL}, and velocity, were combined to give redundant isotope identification of each detected particle. This analysis is similar to that described by Bazin, *et al.*[2], for the study of neutron-rich isotopes using an E/A = 44 MeV ^{86}Kr beam at GANIL.

The detection system was calibrated initially by transporting the primary beam through the device. Further calibration and isotope identification were obtained by setting the A1200 to detect light nuclei and verifying in the ΔE versus time-of-flight isotope spectrum that unbound nuclei such as ^{8}Be and ^{16}F were absent. By collecting data at overlapping rigidity settings, a continuous isotope spectrum was obtained which permitted unambiguous identification. Finally, ΔE, E_{TOTAL}, time-of-flight, and rigidity information from approximately 30 isotopes were fit to determine the energy and time calibrations for the device.

The resulting mass spectra for Z= 30 through 38 (zinc through strontium) are shown in fig. 2. Several new isotopes at or near the proton-drip line are indicated in the mass spectra: ^{61}Ga, ^{62}Ge, ^{63}Ge, ^{65}As, ^{69}Br, and ^{75}Sr. Two events corresponding to ^{60}Ga and one event for ^{70}Kr are also observed; however, it is difficult to conclude from such a small number of events whether these nuclei were in fact identified

or whether the events were due to a background process. The observation of an isotope in the present experiment implies that the ion lives longer than its flight time through the A1200, which is of the order of 150 ns. Therefore it is possible that some of the observed nuclei are actually proton unbound with partial halflives greater than times of this order. The non-observation of an isotope in this work implies either that it has a half life short compared to the flight time or that its production rate was too low to make it observable.

According to the Haustein atomic mass prediction compilation[3] , it is likely that the proton-drip line has now been reached for the odd Z elements arsenic, bromine, and rubidium. An experimental argument for this can be made by integrating the yields of neighboring peaks in the lightest two or three masses of each spectrum in fig. 2. The number of counts in the peaks decreases by roughly a factor of 20 per isotope as the mass decreases. The counts in the ^{65}As peak and the ^{69}Br peak are lower by more than a factor of 100 from the yields of the adjoining isotopes. One interpretation is that these nuclei are very weakly bound and have no excited states and hence in a statistical process would be weakly populated. A case can be made that ^{74}Rb is the last bound nucleus since there are several hundred counts in its peak, and there is not a single event attributable to ^{73}Rb. This is consistent with the previous results of D'Auria *et al.*[4], at ISOLDE. Therefore, ^{69}Br is most likely the highest observable odd–Z $T_Z = -\frac{1}{2}$ nucleus.

In summary, the proton-drip line has apparently been reached for Z=33, 35, and 37, and the heaviest odd–Z $T_Z = -\frac{1}{2}$ nucleus, ^{69}Br, has been identified. Future work is necessary to determine the halflives, decay modes, and structures of these nuclei as well as to continue mapping the proton-drip line above Z=30. A more complete discussion of these results and their implications in certain astrophysical models can be found in reference 5.

a. IPN, Orsay.

References

1. F. Pougheon, *et al.*, Z. Phys. A327 (1987), p 17.
2. D. Bazin, *et al.*, Nucl. Phys. A515 (1990), p 349.
3. 1986-1987 Atomic Mass Predictions, ed. P.E. Haustein, Atomic Data and Nuclear Data Tables 39(1988), p 185.
4. J.M. D'Auria, *et al.*, Phys. Lett. 66B (1977), p 233.
5. M.F. Mohar, *et al.*, Phys. Rev. Lett. 66(1991), p 1571

CALCULATION OF PROJECTILE BREAKUP CROSS SECTIONS IN SINGLE PARTICLE TRANSFER REACTIONS

G. Yoo, G.M. Crawley and J.S. Winfield

The study of single particle stripping reactions to highly excited states is often complicated by the existence of a broad continuum [1,2] (figs.1a, 2a) which likely arises from breakup of the incident projectile. There are numerous approaches [3 – 7] to calculating such breakup processes. We describe calculations and comparisons with data for two such approaches, the Serber model [5], since this has been used commonly in the past, and a more recent approach due to Bonaccorso and Brink. [3,4]

In calculating the cross sections with the Serber model, a plane wave is used both for the external wave function and for the relative wave function of the constituents in the projectile. The target is assumed to be transparent to the breakup fragments and the coulomb and spin-spin interactions between the target and the projectile are neglected. The residual nucleus and the ejectile are assumed to remain in their ground states after the breakup process. The cross section for the emission of the observed particle can be written as

$$\frac{d\sigma}{d\Omega_x dE_x} = N_x m_x (2m_x E_x)^{\frac{1}{2}} |\phi(\vec{p})|^2 \rho(E_x) \tag{1}$$

where

$$\phi(\vec{p}) = \frac{1}{h^{\frac{3}{2}}} \int \phi(r) exp(-\frac{i}{\hbar}\vec{p}\cdot\vec{r}) d^3r \tag{2}$$

is the Fourier transform of the relative wave function of the constituents in the projectile, N_x, m_x and E_x are the normalization constant, the mass and the kinetic energy of the observed particle, respectively. $\vec{p} = \vec{p_o} - \vec{p_x}$ where $\vec{p_x}$, $\vec{p_o}$ are the final momentum of the ejectile and its initial momentum in the projectile in the C.M. frame and $\rho(E_x)$ is the density of the final states. A wave function [8,9] of the Eckart form

$$\phi(r) = C(\frac{\alpha}{2\pi})^{\frac{1}{2}} \frac{e^{-\alpha r}}{r}(1 - e^{-\beta r})^4 \tag{3}$$

is used for the relative wave function of the constituents in the projectile, where $\alpha = (2\mu\epsilon)^{\frac{1}{2}}/\hbar$ with μ and ϵ being the reduced mass and separation energy, and C is a normalization constant. The parameter β is determined by fitting the elastic electron scattering data on the projectile. Even though the Serber model explained the projectile breakup background very well in light ion induced nuclear reactions [8,9,10], it does not explain the background in the reactions $^{208}Pb(^{20}Ne,^{19}Ne)$ and $^{90}Zr(^{20}Ne,^{19}Ne)$ at incident energies

of 25, 30 and 40 MeV/u. One reason is that this model treats only elastic and direct breakup process, whereas a heavy target or a heavy projectile can be excited by inelastic scattering and sequential breakup processes may not be negligible. Another reason is that the only characteristics of the particles which are considered are the momenta transferred and the masses, whereas breakup processes depend also on the coulomb and spin-spin interactions and the angular momentum transferred.

In the Bonaccorso-Brink model [3,4], the cross sections are calculated both for transitions to compound nucleus states and to continuum states, which correspond to a projectile breakup process. In this model, it is assumed that a nucleon makes a transition from a single particle state ψ_i with angular momentum L_i, J_i and energy ϵ_i in the first nucleus to a continuum state ψ_f with angular momentum L_f, J_f and energy ϵ_f in the final nucleus. The input values of the initial state are determined by the characteristics of the nucleon being transferred. The cross sections for a transiton to a continuum state and to a compound state are given by

$$\frac{d\sigma}{d\epsilon_f} = \pi \frac{R_s - a_c}{\eta} \sum_{l_f=0}^{l_{max}} \left(|1 - S_{l_f}(\epsilon_f)|^2 + 1 - |S_{l_f}(\epsilon_f)|^2 \right) B(l_f, l_i) \tag{4}$$

where $B(l_f, l_i)$ is an elementary transition probability from initial state ψ_i to final state ψ_f, $S_{l_f}(\epsilon_f)$ is a S-matrix element for elastic scattering of a nucleon with energy ϵ_{l_f} by the target, R_s is a strong absorption radius, a_c is a coulomb length parameter and η is a z component of the momentum of the transferred nucleon relative to the initial and final nuclei. The first term is due to the elastic scattering of the transferred nucleon by the target nucleus, which is a transition to a continuum state, while the remaining term is due to compound nucleus formation and includes all the excitations of the target after the reactions. The S-matrix elements are dependent on the incident particle's energy and are obtained from a DWBA calculation for the nucleon elastic scattering reaction on the appropriate targets. We can also apply this method to calculate the transition cross sections multinucleon, and can be calculated by using effective binding energies, Q-values and normalization constants.

There are two aspects of this model which should be noted. One is the sensitivity of the results to the choice of the optical parameters and the other is the dependence on the details of the initial state. The optical model parameters were taken from Mahaux and Sartor [11], where the volume imaginary and surface strength are parameterized in closed form. The strength of the real and spin-orbit potentials are chosen

Reactions	$E_{lab}(^{20}Ne)$ (MeV)	Initial State	L_i	J_i	L_f^{max}	Spectroscopic Factor
$^{90}Zr(^{20}Ne,^{19}Ne)$	500, 600, 800	$1p_{1/2}$	1	0.5	30	1.96
$^{208}Pb(^{20}Ne,^{19}Ne)$		$2s_{1/2}$	0	0.5	30	0.56
		$1d_{5/2}$	2	2.5	30	1.06

Table 1: Input Parameters for Bonacccorso-Brink Model

to reproduce the position of the known bound and resonance states of the target. The input parameters for calculating the transition cross sections using Bonaccorso-Brink model are given in table 1 and the results are given in Figs. 1 and 2 for the reactions $^{208}Pb(^{20}Ne,^{19}Ne)^{209}Pb$ and $^{90}Zr(^{20}Ne,^{19}Ne)^{91}Zr$ at $E_{inc} = 800, 600$ and $500MeV$. The dashed curve corresponds to the elastic break-up spectrum. The dotdashed curve is the sum of break-up plus absorption and should correspond to the experimental spectra. In Fig.1.(a), the first bump at $\varepsilon_f = 4MeV$ ($E_x = 7.9MeV$) is due mainly to low-lying resonance states in ^{209}Pb. The $1k_{17/2}$ state contributes 49% to the peak cross section, the $1j_{13/2}$ contributes 12%, the $2h_{11/2}$ gives 5% and finally 10% is due to the $1i_{19/2}$ resonance. It is interesting to note that in this region of excitation energy there is very little breakup predicted. There is also a large bump at higher excitation energy centered at $19MeV$. Again most of the strength predicted arises from high lying resonance states such as the $1i_{19/2}$, the $1l_{21/2}$ and the $1m_{23/2}$ states. Similar spectra are predicted at 600 and 500 MeV incident energy but the breakup contribution is even less. The general trend of the data for both ^{208}Pb and ^{90}Zr targets shown in Figs. 1 and 2 is predicted reasonably well by these calculations. One caution is that the predictions are for the total cross sections and the spectra are taken at a particular angle. It would be useful to have angle dependent predictions to compare more directly with the measured spectra.

The shape of the predicted spectra is very sensitive to the details of the initial state. In ^{20}Ne there are three states from which the neutron can be transferred, the $2s_{1/2}$ $1p_{1/2}$ $1d_{5/2}$. The theoretical contributions of the s, p and d states at the three incident energies are shown in Fig.1.(b) and Fig.2.(b). The full curves are at $500MeV$, the dashed curves at $600MeV$ while the dotted curves are at $800MeV$. The $2s_{1/2}$ state has a much larger magnitude with respect to the $1p_{1/2}$ and $1d_{5/2}$ due to its large asymptotic normalization constant. The shape of the spectra for the d initial state changes little with the incident energy. Only the magnitude varies. In contrast, the shape of the spectra for the s and p initial states changes markedly and the second bump centered at $19MeV$ appears as the incident energy is increased.

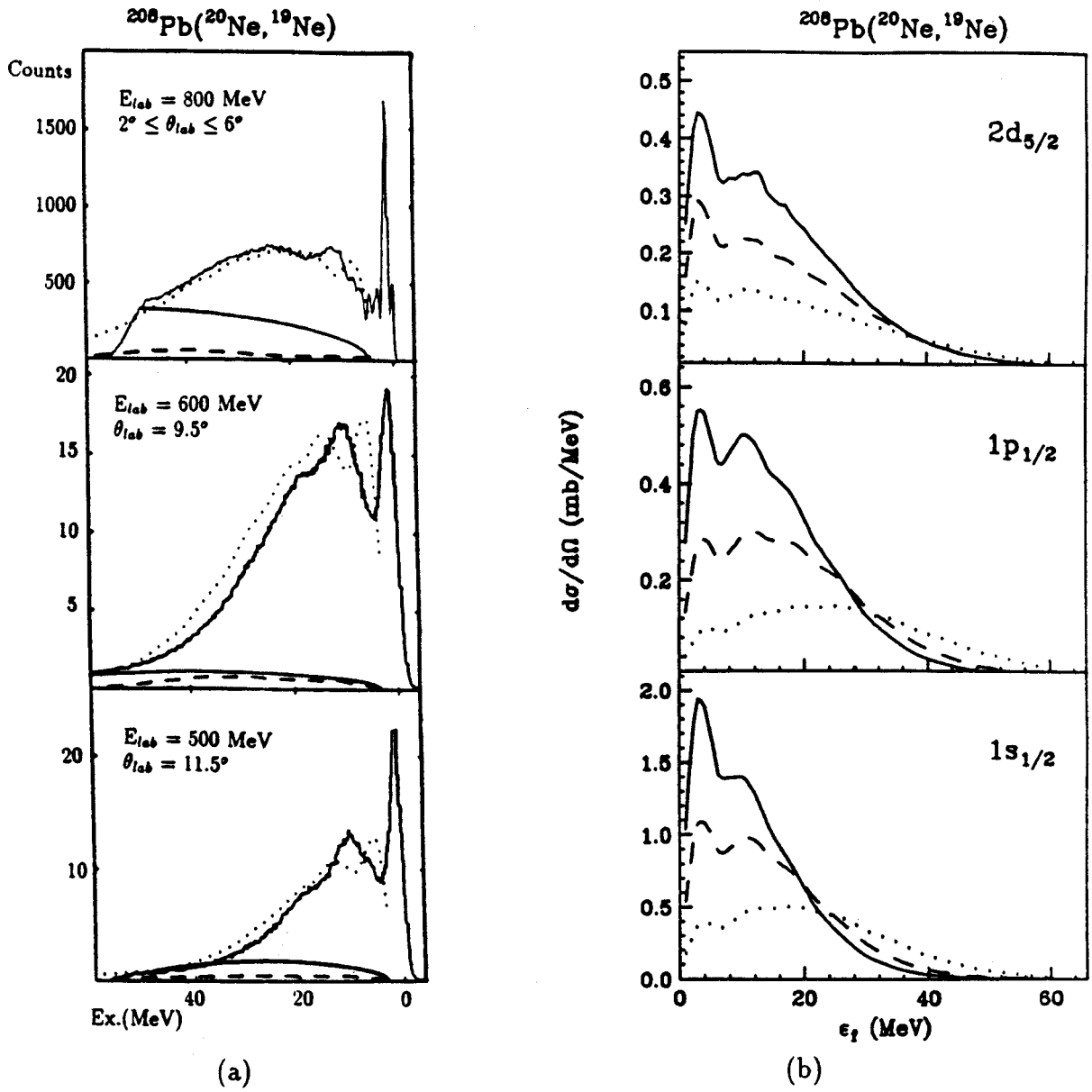

Figure 1: (a). Spectra of the $^{208}Pb(^{20}Ne,^{19}Ne)$ reaction at 500, 600 and 800 MeV with theoretical calculations. The solid lines show Serber model calculations, the dashed lines Bonaccorso-Brink model calculations of the transition to continuum state. The dotted lines show the total transition. (b). Calculations of the total transition cross sections for the reaction $^{208}Pb(^{20}Ne,^{19}Ne)$ at 500,600 and 800 MeV showing the s, p and d contributions separately.

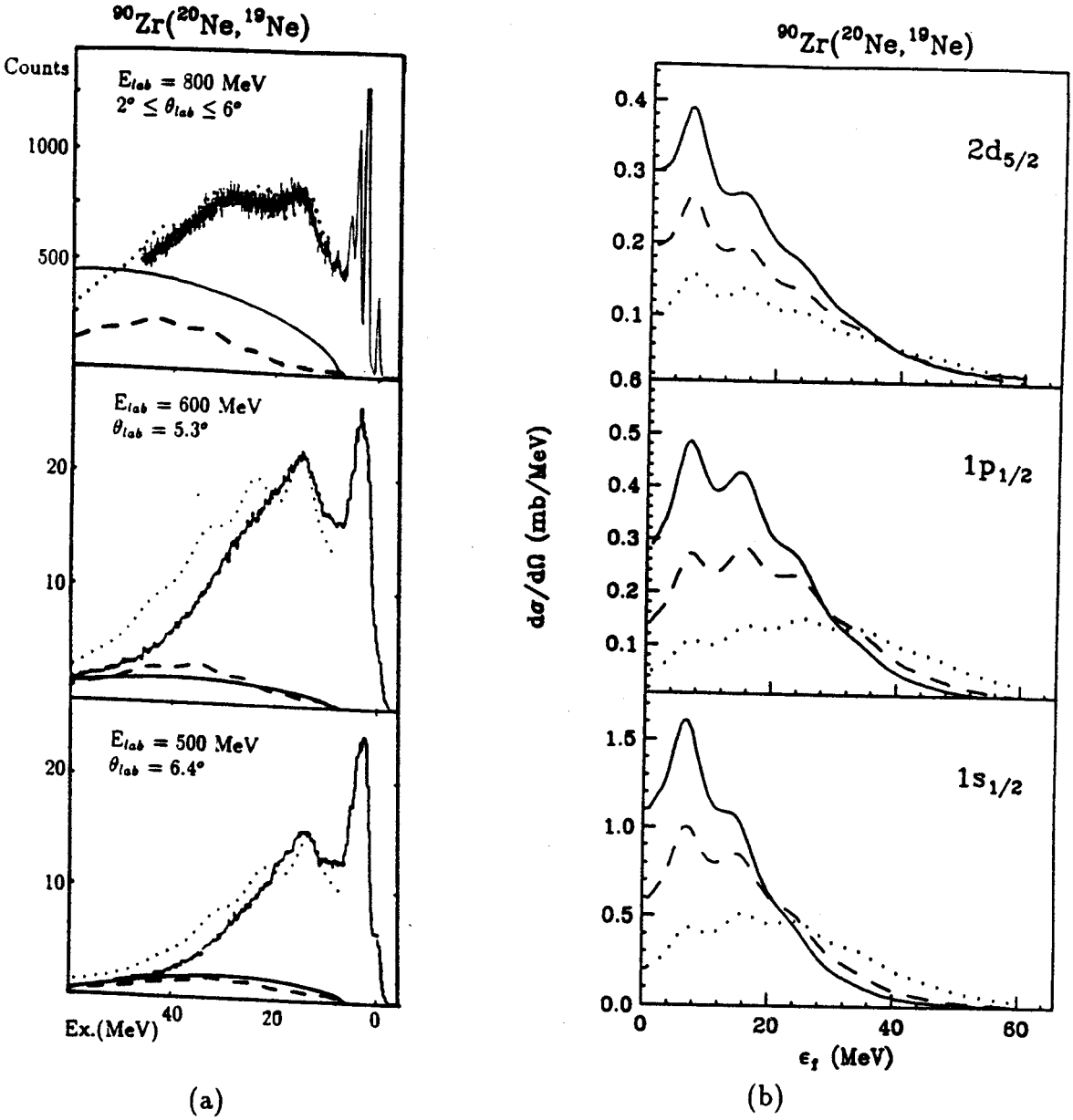

Figure 2: (a). Spectra of the $^{90}Zr(^{20}Ne,^{19}Ne)^{91}Zr$ reaction at 500,600 and 800 MeV with theoretical calculations. The solid lines show Serber model calculations, the dashed lines Bonaccorso-Brink model calculations of the transition to continuum state. The dotted lines show the total transition. (b). Calculations of the total transition cross sections for the reaction $^{90}Zr(^{20}Ne,^{19}Ne)$ at 500,600 and 800 MeV showing the s, p and d contributions separately.

One approach planned to cast more light on this problem is to carry out a coincidence experiment with the reaction $^{90}Zr(^{7}Li,^{6}He\,p)$ where the ^{6}He particles are detected at forward angles and the protons in an array at backward and forward angles. Coincidences of the ^{6}He particles with protons detected at backward angles should select only the spectra corresponding to resonance states and should eliminate the breakup part of the spectrum, since the protons arising from the breakup of ^{7}Li will be restricted to forward angles. Further experiments to clarify these issues are in progress.

The authors would like to thank Drs Angela Bonaccorso and David Brink for valuable discussions on this work.

References

1. S. Fortier et al., Phys. Rev. C41 (1990), p 2689.
2. N. Frascaria et al., IPN Orsay, Rapport Annuel (1987), p 41.
3. A. Bonaccorso and D.M. Brink, Phys. Rev. C38 (1988), p 1776.
4. A. Bonaccorso and D.M. Brink, private communication and Phys. Rev. to be published, 1990.
5. R. Serber, Phys. Rev. 72 (1947), p 1008.
6. L. Lo Monaco and D. M. Brink, J. Phys. G11 (1985), p 935.
7. Fl. Stancu and D. M. Brink, Phys. Rev. C32 (1985), p 1937.
8. J.R. Wu et al., Phys. Rev. C20 (1979), p 1284.
9. N. Matsuoka et al., Nuclear Phys. A311 (1978), p 173.
10. R.J. de Meijer et al., Rev. Mod. Phys. 57 (1985), p 147.
11. C. Mahaux and R. Sartor, Nuclear Phys. A493 (1989), p 157.

ROTATIONAL BANDS IN ^{174}Re

W. A. Olivier, W.-T. Chou,* A. Rios, C. V. Hampton, Wm. C. McHarris, and R. Aryaeinejad[a]

Odd-odd Re nuclei present an interesting challenge for in–beam γ–ray spectroscopy. The characterization of rotational bands in ^{174}Re continues a series of studies of neutron–deficient members of this set.[1] While the rotational structure of this nucleus has been elusive in previous attempts at characterization, present data have allowed us to assign two rotational bands, consisting of seventeen levels, to ^{174}Re.

We studied the ^{159}Tb(^{20}Ne,5$n\gamma$) and ^{139}La(^{40}Ar,5$n\gamma$) reactions at NSCL and the ^{165}Ho(^{16}O,7$n\gamma$) reaction at SUNY Stony Brook – NSL. From these diverse reactions we have identified γ–ray transitions in two rotational bands. These include the "doubly–decoupled" band, characteristic of many of the odd–odd Re nuclei[2]; it consists of coupling the $\pi h_{9/2}$ 1/2$^-$ orbital and a ν 1/2$^-$ orbital. In addition, a second band, plausibly built on a coupling with the $\pi h_{11/2}$ 9/2$^-$ orbital, was populated. Figure 1 depicts the partial level scheme for ^{174}Re. Because of poor statistics, the level schemes have not been extended to greater excitation energies commonly seen in neighboring nuclei.

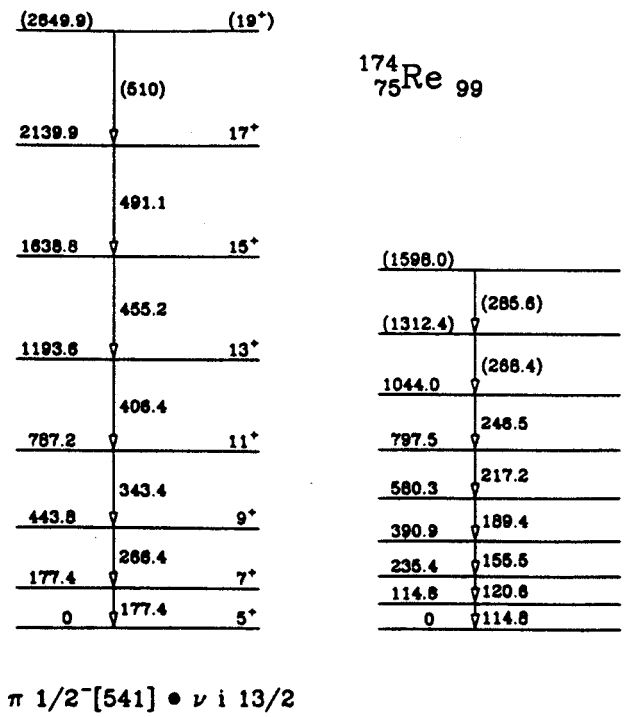

Figure 1: Partial level scheme for ^{174}Re showing the "Doubly–decoupled" band and a ΔI=1 band.

A typical gated spectrum can be seen in figure 2. This spectrum illustrates a rather abrupt

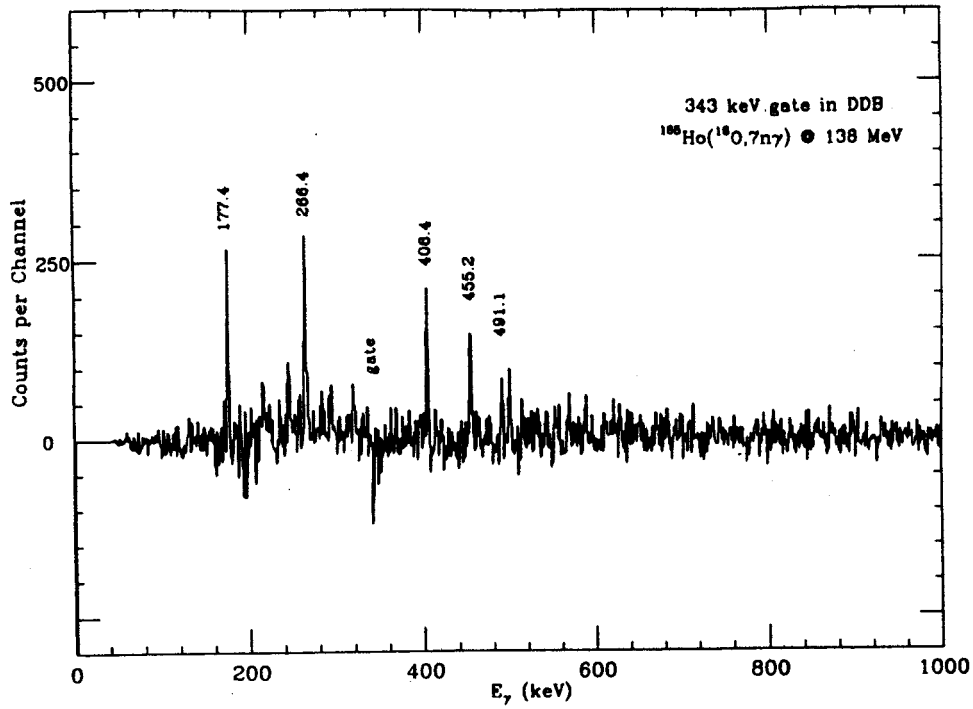

Figure 2: Coincidence spectrum gated on the 343 keV transition in the doubly–decoupled band in ^{174}Re.

termination of the observable transitions in the band due to lack of statistics.

One of the fundamental ambitions of these studies is to understand more about p-n interactions in fairly massive systems. The high correlation between the doubly–decoupled band level spacings and those in the analogous "core" nuclei offer encouragement towards this end. In addition, the general behavior of alignment of particle and core angular momentum in these systems may offer a microscopic explanation of the basis of superdeformation.[3]

a. INEL/EG&G, Idaho Falls, ID 83415
* Present Address: Physics Department, Brookhaven National Laboratory, Upton, NY 11973

References

1. W.-T. Chou et al., MSU-NSCL Annual Report 1989, p 85.
2. W.A. Olivier et al., *Exotic Nuclear Spectroscopy*, Wm.C. McHarris, ed. (1990), p 397.
3. W.A. Olivier et al., MSUCL-763 report (1991).

IN-BEAM γ-RAY SPECTROSCOPY OF HIGH SPIN STATES IN ^{175}Re

W. A. Olivier, W.-T. Chou,* A. Rios, C.V. Hampton, Y. Dardenne, Wm. C. McHarris, R. Aryaeinejad[a], Y. Liang[b], R. Ma[b], E.S. Paul,[b,†] and N. Xu[b]

An in–beam γ–ray spectroscopic study was performed at SUNY Stony Brook–NSL as a continuation of a series of investigations of lighter mass Re nuclei.[1 – 3] γ-γ coincidence and angular distribution data were used to investigate the rotational band structure in the previously uncharacterized ^{175}Re nucleus. Four rotational bands comprised of forty-eight levels were identified. These consist of a decoupled band built on the $h_{9/2}$ 1/2$^-$[541] proton state, a highly-compressed band built on the $h_{11/2}$ 9/2$^-$[514] state, a highly-deformed quasi-particle band associated with the $h_{9/2}$1/2$^-$[541] state and a more normal band built on the $d_{5/2}$ 5/2$^+$[402] state. The decoupled band exhibits a rotational alignment at 0.315 MeV, consistent with neighboring odd-mass Re nuclei. Experimental results are compared with theortical calculations in the IBA framework.

The ^{175}Re nucleus has been a conspicuous gap in the data for the lighter odd–mass Re nuclei, with the structures of ^{171,173,177,179}Re having been characterized by several groups.[4, 5, 6, 7] The identification and analysis of the rotational band structure in ^{175}Re is consistent with the neighboring odd–mass Re nuclei and a preliminary report by Reidinger, et al.[8] It indicates that, while the fermi surface is highly sloped for valence proton orbitals, general features of the rotational bands remain unchanged throughout this series of nuclei. Re nuclei are of particular interest because they lie in a region where the Nilsson orbitals exhibit large driving effects on the nuclear shape, presenting the strong possibility of shape coexistence. For example, population of the strongly decoupled $\pi h_{9/2}$1/2$^-$[541] state is a strong driving force to higher deformations whereas the population of the $\pi h_{11/2}$9/2$^-$[514] state has a moderate propensity for driving toward more spherical shapes. An understanding of the population preferences of these types of states will lead to better understanding of the reaction mechanisms and specific nuclear structure.

High–spin states in ^{175}Re were populated in studies using two heavy–ion induced reactions at Michigan State University–NSCL and one at SUNY Stony Brook–NSL. γ–rays were observed with similar detection systems in the two studies at MSU. The reactions were ^{159}Tb(^{20}Ne,4$n\gamma$) at 105 MeV and ^{139}La(^{40}Ar,4$n\gamma$) at 192 MeV. The detection systems consisted of two 15% efficient coaxial HPGe detectors at $\pm$90° with respect to the beam. The detectors were shielded with large NaI(Tl) annuli and 5 to 8 — 7.6×7.6 cm NaI(Tl) detectors were clustered about the target as a multiplicity filter. In the second study

a planar LEPS was also added at 35°. Both of these studies yielded good results but were lacking in statistics as a result of the large distance between the target and the detectors mandated by the size of the NaI(Tl) annuli.

The third study of the ^{175}Re system, conducted at SUNY Stony Brook–NSL, used the ^{165}Ho(^{16}O,6$n\gamma$) reaction with a 138 MeV ^{16}O beam from the NSL tandem–superconducting linac. A thick target was used to maximize the production of the products and to attenuate product migration, which leads to doppler broadening. The γ–ray detection was performed with an array of four HPGe detectors compton shielded with Stony Brook's standard transverse BGO shields.[9] Better statistics were observed in this study primarily as a result of the reduced detector–to–target distance allowed by the BGO shields. Data was analyzed off-line in a similar fashion for each experiment, using various stripping and peak fitting codes.

In each of the three experiments, we observed very strong population of a "decoupled" band built on the $h_{9/2}1/2^-$[541] proton state. Figure 1a. shows a representative "singles" (requiring the firing of one to three multiplicity hit detectors) spectrum of the detectors used in the ^{165}Ho(^{16}O,6$n\gamma$) reaction at Stony Brook. The most intense transitions observed are those belonging to this decoupled band. These energies are labeled in the figure. Most of the contaminant lines in this spectrum come from other Re isotopes produced in the thick target. However, stringent gating requirements and calculated integrated thick–target excitation functions eliminated most of the resulting difficulties for the anaysis.

The second most intensely populated rotational band is built on the $h_{11/2}9/2^-$[514] state. The energies of the transitions in this band are labeled in the singles spectrum from the ^{139}La(^{40}Ar,4$n\gamma$) reaction shown in fig. 1b. This band is a common feature in the light odd–mass Re nuclei from ^{171}Re to all the way up to stability at ^{186}Re. Its existence demonstrates the suprisingly stable nature of the fermi surface throughout the region.

Representative gated coincidence spectra are shown in fig. 2. These depict the other two bands observed in this study. Figure 2*a* is a gate on the quasi–particle band associtated with the $h_{9/2}$ state. Figure 2*b* is a gate on a transition in the $d_{5/2}$ band. This band is considered to be the ground state in some of the other odd–mass Re nuclei, but we see no evidence of this in the ^{175}Re case.

The level scheme for the observed bands is shown in fig. 3. The energies of the bandheads relative

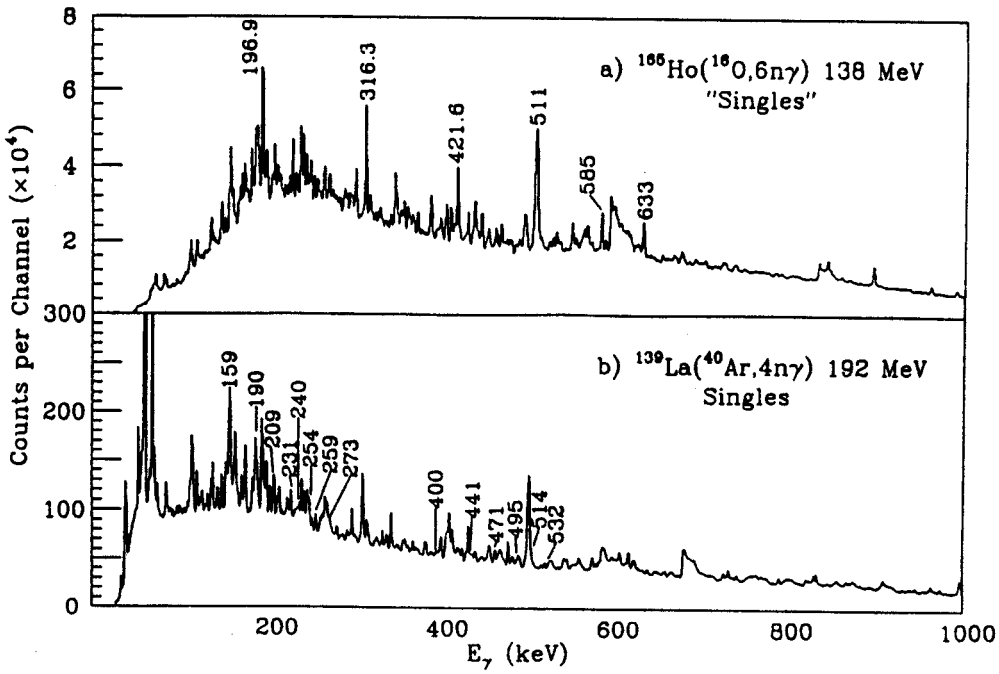

Figure 1: ^{175}Re singles γ–ray spectrum showing the two most prominent rotational bands. For clarity, transitions in different bands are labeled in the two parts of the figure, although transitions from both bands appear in each half. *a*) A "singles" spectrum (requiring the firing of 1 to 3 BGO hit detectors in a multiplicity filter) from the ^{165}Ho(^{16}O,6$n\gamma$) reaction; the labeled transitions originate from the decoupled band based on the $\pi h_{9/2}1/2^-$[541]state. *b*) A singles spectrum from the ^{139}La(^{40}Ar,4$n\gamma$) reaction; here the labeled transitions originate from the highly-compressed band based on the $h_{11/2}9/2^-$[514] state.

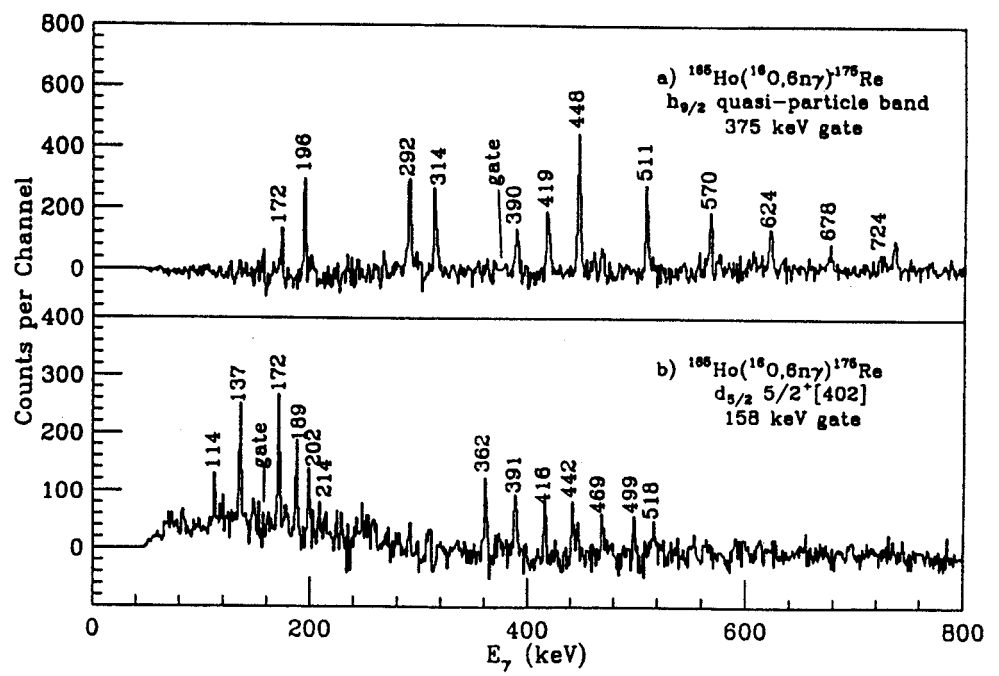

Figure 2: Representative gated spectra showing transitions in *a*) $h_{9/2}$ 1/2$^-$[541] quasi–particle band and *b*) $d_{5/2}$ 5/2$^+$[402] band.

to each other are not known, nor can the ground state of the system be specified.

The decoupled band in ^{175}Re illustrates the similarity in population patterns of the different reactions. Figure 4 shows the summed gates of the decoupled bands for the three distinctly different reactions which were studied. In each of the three frames one can observe population of the band up to about spin $49/2^-$. This means one cannot invoke traditional yrast arguments to explain the population. The population of this band is undoubtedly the result of it being the lowest member in a manifold of similar bands populated directly by the heavy-ion reactions. These bands funnel their depopulation down through similar states to the observed band. It is positions of the funneling bands in the lower portion of the multitude of feeding/funneling bands, not directly observed, not the initial band and spin populated that determines the entry into the observed decoupled band.

Theoretical calculations for the ^{175}Re system were carried out in the framework of IBA. Previous IBFA calcuations for this nucleus, while it was still entirely uncharacterized experimentally, were preformed with parameters extrapolated from higher mass Re nuclei.[2] These calculations yielded remarkably good agreement to the experimentally observed structure. Only very minimal changes in the interaction strength parameters from the previous calculations were made in the present calculations. This demonstrates the stength of IBA type calculations to predict structural features for systems without excessive "parameter fitting" actions. Table 1. illustrates the very minimal changes which were affected.

Good agreement between the calculated rotational levels and three of the bands observed experimentally can be seen in fig. 5. The bands spacings in the calculated systems do not exactly reproduce the experimentally observed ones, in part due to the coriolis interactions. These highly-aligned, highly-deformed bands have very strong coriolis contributions which are not specifically damped in the calculations. The effect then, generally is to have more compressed spacings at higher spins in the calculated systems, especially those which have the stronger coriolis influences.

The fourth band characterized in the experiments is not observed in the calculations. This can be attributed to either the fact that it lies higher in energy so that the feasible theoretical states are very highly mixed and thus characterization of the band specifically is difficult at best, or possibly that the band is built on a quasi-particle alignment which can not be described in the framework of the IBFA in which the calculations were conducted. The latter explaination seems more likely given the very strong feeding to the $h_{9/2}$ band observed in the experimental studies.

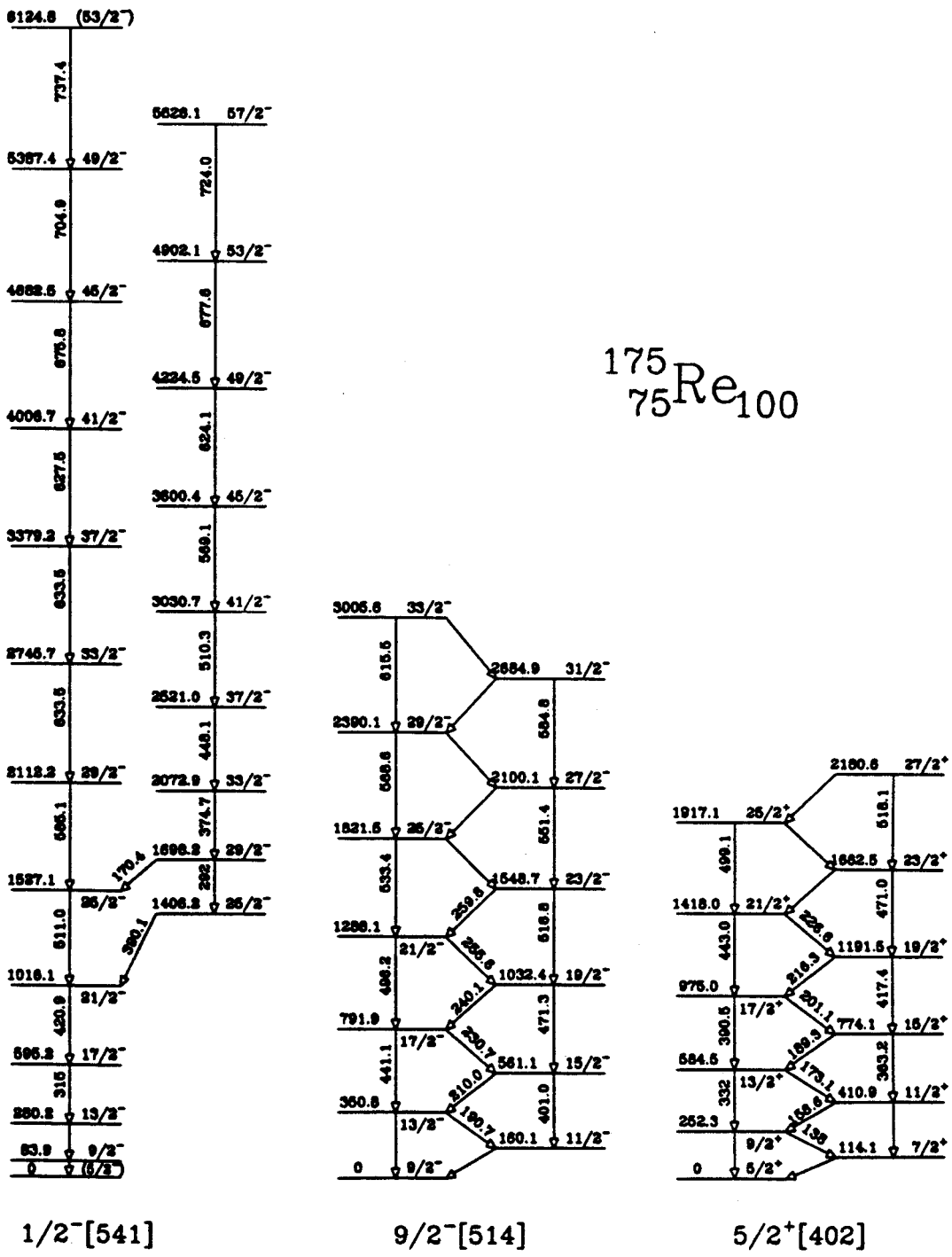

Figure 3: Level scheme of ^{175}Re showing the four rotational bands characterized in these experiments.

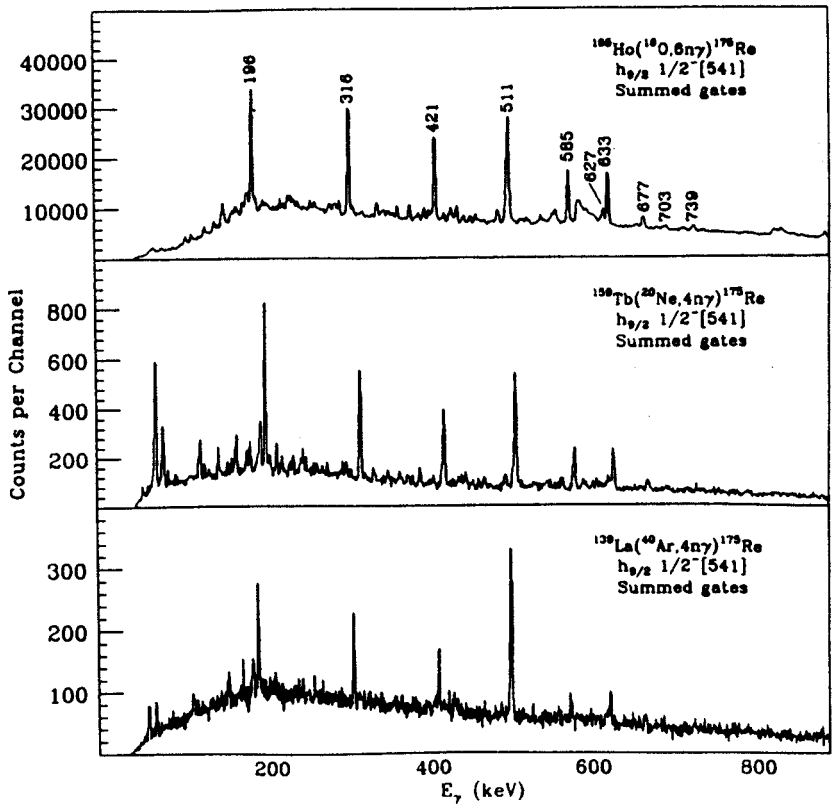

Figure 4: Comparison of the best summed gated spectra for the decoupled band in ^{175}Re. These spectra demonstrate that the population pattern into this low-Ω band which was most strongly populated in each reaction, is basically independent of the angular momentum brought in by the projectile.

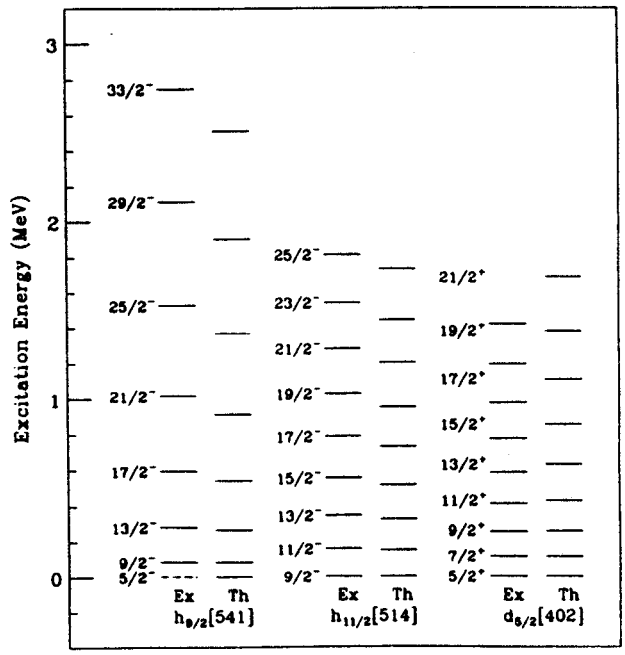

Figure 5: Comparison of Interacting-boson-fermion approximation (IBFA) calculations to three of the experimentally observed bands in ^{175}Re.

Table 1.

Comparison of extrapolated (Previous) parameters to experimentally fit (Present) parameters.

Parameter	Previous	Present	% change
	Negative-parity states		
Λ_0^-	1.28	1.28	0
Γ_0^-	1.25	1.25	0
A_0^-	-0.10	-0.10	0
χ	-1.20	-1.20	0
$\nu^2 h_{11/2}$	0.58	0.58	0
$\nu^2 h_{9/2}$	0.05	0.05	0
$E(MeV)h_{9/2}$	5.20	5.20	0
	Positive-parity states		
Λ_0^+	0.295	0.272	-8
Γ_0^+	0.751	0.772	-3
A_0^+	0.05	0.00	-100
χ	-1.20	-1.20	0
$\nu^2 g_{7/2}$	0.974	0.974	0
$\nu^2 d_{5/2}$	0.919	0.919	0
$\nu^2 d_{3/2}$	0.722	0.772	0
$\nu^2 s_{1/2}$	0.705	0.705	0

In the present study of ^{175}Re we have characterized four rotational bands consisting of forty-eight levels. The most intensely populated is the decoupled band based on the $h_{9/2}$ orbital. We have demonstrated the power of IBA type calculations on the fringes of regions that are well characterized not only to reproduce good fits to the experimentally observed data, but also as a predictive tool.

a. INEL/EG&G, Idaho Falls, ID 83415
b. SUNY Stony Brook, Stony Brook, NY 11794
* Present Address: Physics Department, Brookhaven National Laboratory, Upton, NY 11973
† Present Address: Oliver Lodge Laboratory, Univ. of Liverpool, P.O. Box 147, Liverpool L69 3BX, UK

References

1. M.F. Slaughter, et al., Phys. Rev. C 29 (1984), p 114.
2. W.-T. Chou, Ph.D. Thesis, Michigan State University, 1989 (unpublished).
3. W.A. Olivier, et al., *Exotic Nuclear Spectroscopy*, Wm.C. McHarris, ed. (1990), p 397.
4. R.A. Bark, et al., J. Phys. G 15 (1989), p L169.
5. R.A. Bark, et al., Nucl. Phys. A501 (1989), p 157.
6. W. Waluś, et al., Phys. Scr. 34 (1986), p 710.
7. Ts. Venkova, et al., Z. Phys. A. 334 (1989), p 385.
8. L. Riedinger, et al., Nucl. Phys. A520 (1990), p 287c.
9. L. Hildingsson, et al., Nucl. Instr. and Meth. A252 (1986), p 91.

ROTATIONAL BANDS AND POSSIBLE SUPERDEFORMATION IN ^{132}Pr

C.V. Hampton, J.E. Johnson, Aracelys Rios, W.A. Olivier, R.M. Ronningen, Wm.C. McHarris, R. Aryaeinajad [a], and ORNL Nuclear Structure Research Group.

Results from a fusion-evaporation experiment conducted at the Holifield Heavy Ion Research facility at Oak Ridge National Lab are presented. The objective of the study is to investigate the proton-neutron residual interaction in an odd-odd system in the A = 130 region. We have chosen to determine the rotational band structure of ^{132}Pr at high spin and to search for superdeformation in this nucleus. Superdeformed rotational bands (SD) have been reported for other nuclides in this region: ^{132}Ce [1], Nd isotopes [2], ^{130}La [3], and ^{131}Ce [3]. Such SD bands have the properties of deformed prolate rotors (β = 0.35-0.4) and have been observed in this region only at high spin. They appear to originate from highly deformation-driving intruder orbitals based on at least one $i_{13/2}$ neutron. Other N = 73 isotones exhibit superdeformation, so $^{132}Pr_{73}$ is a good candidate.

A ^{37}Cl beam from the HHIRF Tandem Van de Graaff accelerator was directed onto a thin target of isotopically enriched ^{100}Mo to produce the compound nucleus ^{137}Pr*. Excitation functions using a "Cascade" calculation predict the population of at least eight different reaction channels. A 160-MeV beam was chosen to enhance the lower intensity states in the 5n evaporation channel for ^{132}Pr. The γ-rays emitted during the reaction were detected using the compton-suppression spectrometer – 21 detectors arranged in a 4π dodecahedron geometry. Each detector unit consists of a Ge crystal, a BGO catcher, and either a BGO or NaI compton shield. The electronics were arranged so that triple coincidence events were collected ($\approx$1000/s) onto tape. Data were sorted by a prescan technique (using HHIRF software) into gain- and doppler-shifted and time-corrected events. Two dimensional histograms of energy vs time were scanned into 2000 × 1500 arrays. By placing energy gates on the 2D histogram, TAC spectra were produced from which the lifetimes of the states could be calculated. Time gates produced prompt and delayed total energy spectra for each detector, along with background spectra contributed by the nuclide activities and x-ray peaks from the Pb frame surrounding the target. Approximately 250 million coincidence events have been scanned into 2900 × 2900 E vs E arrays. From these time-gated 2D histograms, coincidence spectra for both prompt and delayed regions were produced. Rotational band transition energies have been deduced from these single-gated spectra.

The observed rotational bands confirm that the 160-MeV reaction populated the 5n, 4n, 3n, and

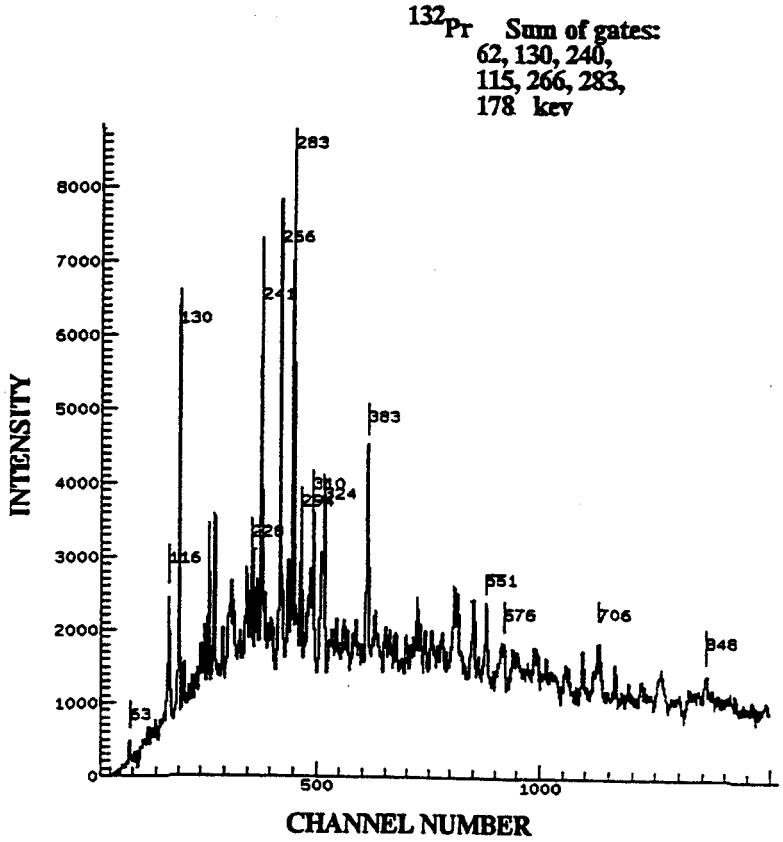

Figure 1: Gated spectrum obtained from the 160 MeV ^{37}Cl on ^{100}Mo reaction.

possibly the $2n$ evaporation channels producing ^{132,133,134,135}Pr, as well as the $p4n$ and $p3n$ channels producing ^{132,133}Ce and the $\alpha 4n$ and $\alpha 3n$ channels for ^{129,130}La. Figure 1 shows the summed, single-gated spectrum for ^{132}Pr. Figure 2 shows corresponding spectra for a few other of these nuclei. During the experiment no attempt was made to filter out any reaction channel, for this might have also reduced the contribution from ^{132}Pr. (The mechanism for producing SD bands in optical yields is still not well understood. In the ^{152}Dy region they appear to be produced best by relatively "cold" compound nuclei, but this is not necessarily true in the Ce-Pr region.) This approach appears to be correct, since SD bands have been observed in nuclei in this region at intensities of 1-10%, and the previously identified[1] SD band in ^{132}Ce was clearly observed in the present study. (See Figure 2a. Arrows mark SD transitions.)

The coincidence spectra for ^{132}Pr, in general, confirm the three bands observed in a previous (low-spin) study[4] using the ^{117}Sn(^{19}F, $4n\gamma$)^{132}Pr reaction. We have observed a few differences: The relative intensities of the $\Delta I = 1$ and the intensities of the $\Delta I = 2$ signatures of the yrast $\pi h_{11/2} \otimes \nu h_{11/2}$ band and the $\pi h_{11/2} \otimes \nu g_{7/2}$ band are lower than previously indicated. We have seen additional energy transitions

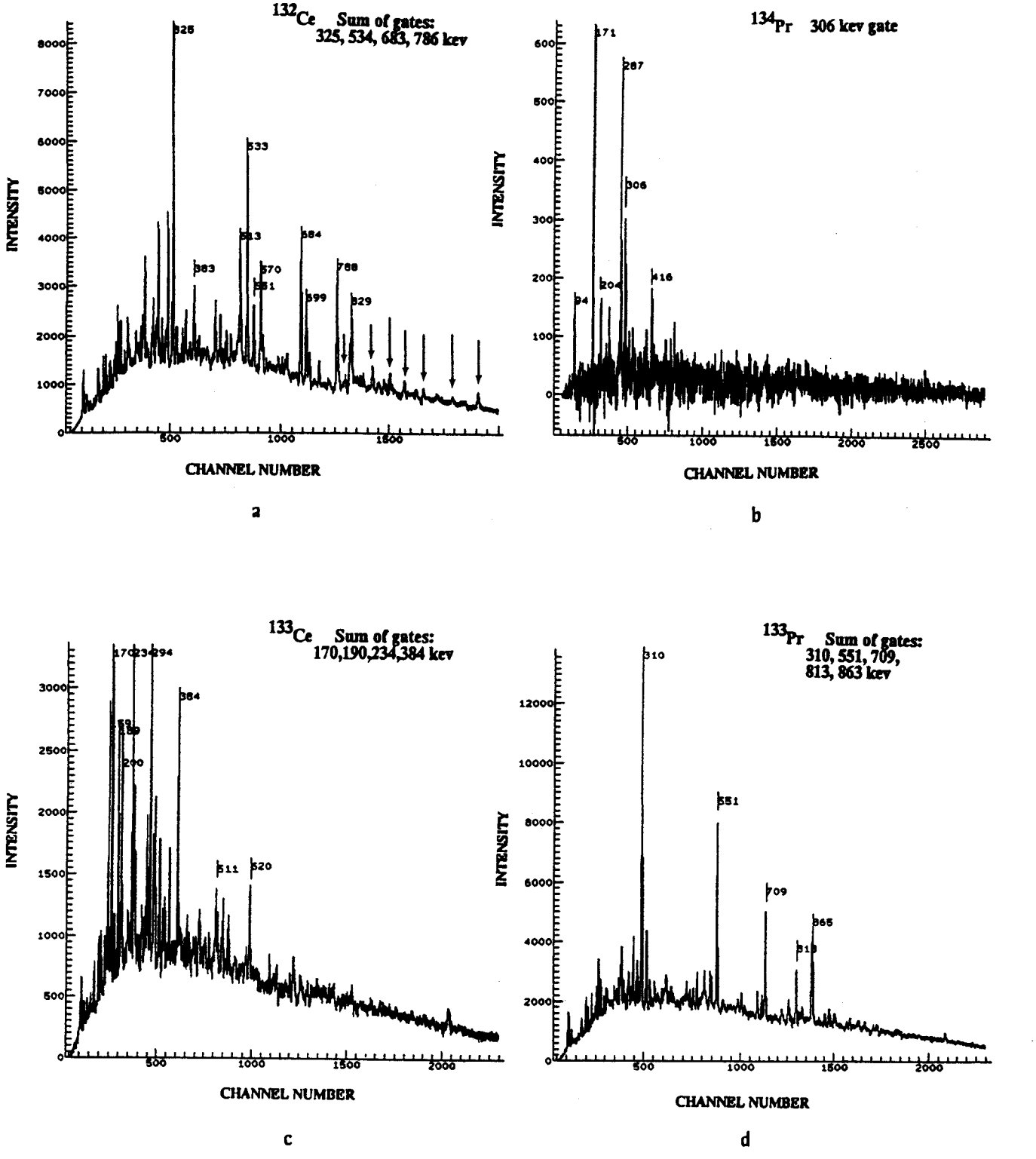

Figure 2: Gated spectra obtained from the 160 MeV ^{37}Cl on ^{100}Mo reaction.

that may extend the rotational band decay scheme to higher spin states. We have found a low-energy transition (62 keV) not seen before that is in coincidence with the yrast band, which may redefine the energy of the ground state. This supports cranked shell-model calculations[4] that suggest this yrast band should begin a few hundred keV below the $\pi h_{11/2} \otimes \nu g_{7/2}$ band.

In the energy region between 325 and 800 keV many low intensity peaks (<10%) can be seen when gated spectra are summed together (see Figure 1). These have not been characterized yet because of the complex nature of the spectra, the low intensities, and the many transition energies that are in common among the different nuclides. This region (where the SD transitions may lie) is interesting in that multiple peaks exist, separated by about 5 keV. There is the possibility that these are actually multiple, low intensity bands with closely related moments of inertia. SD bands of this nature have recently been discovered in the $A \approx 150$ and 190 regions[5,6] and have been attributed to quasiparticle pseudo-spin alignments. In order to establish the presence of SD bands and characterize these low-intensity transitions, the data must be scanned into 2D arrays from which multiple gates can be extracted. We have now reached this stage of of data analysis.

a. Idaho National Engineering Laboratory

References

1. E.M.Beck et al., Phys. Rev. Lett. 58 (1987), p 2182.
2. R. Wadsworth et al., J. Phys G. 13 (1987), p L207.
3. M.J. Godfrey et al., J. Phys G. 15 (1989),p L163.
4. E.S. Paul et al.,Phys. Rev. C37 (1988), p 1478.
5. F.S. Stevens, Nucl. Phys. A520 (1990), p 91c.
6. F. Azaiez et al., Phys. Rev. Lett. 66 (1991), p 1030.